Resonant cavity enhancement in heterojunction GaAs/AlGaAs terahertz detectors

Esaev, D. G.; Matsik, S. G.; Rinzan, M. B. M.; Perera, A. G. U.; Liu, H.; Buchanan, M.

published in
Journal of Applied Physics
2003

DOI (link to publisher)
10.1063/1.1539918

document version
Publisher's PDF, also known as Version of record

Resonant cavity enhancement in heterojunction GaAs/AlGaAs terahertz detectors

D. G. Esaev, S. G. Matsik, M. B. M. Rinzan, and A. G. U. Perera[a)]
Department of Physics and Astronomy, Georgia State University, Atlanta, Georgia 30303

H. C. Liu and M. Buchanan
Institute for Microstructural Sciences, National Research Council, Ottawa K1A 0R6, Canada

(Received 7 October 2002; accepted 27 November 2002)

The room-temperature absorption and reflection spectra in the range of 5–100 μm (3–60 THz) for multilayer heterojunction interfacial work function internal photoemission (HEIWIP) GaAs/AlGaAs far-infrared (FIR) detectors are presented. Calculated results based on the free carrier absorption and interaction with optical phonons are found to be in good agreement with the experimental results. Experimental responsivity spectra demonstrate the expected maxima from the absorption measurements due to resonant cavity effects. It is shown that the resonance cavity architecture enhances the performance of the FIR HEIWIP detectors and further improvement is proposed through the use of n^{++} and p^{++} bottom contact layers or doped substrates. © *2003 American Institute of Physics.* [DOI: 10.1063/1.1539918]

I. INTRODUCTION

High performance far-infrared (FIR) (20–200 μm) detectors are needed for various space astronomy applications such as the airborne mission of the National Aeronautics and Space Administration Stratospheric Observatory for Infrared Astronomy and the European Space Agency's Hershel Space Observatory. Traditional Ge (stressed or unstressed) and Si or Ge blocked impurity band detectors have been used as FIR detectors for decades.[1] Homojunction interfacial work function internal photoemission infrared photodetectors based on Si or GaAs were studied as alternative detectors.[1] Recently, a modification using a heterojunction to obtain the work function instead of band gap narrowing was suggested giving the heterojunction interfacial workfunction internal photoemission (HEIWIP) infrared photodetector.[2] HEIWIP's have the advantage of allowing reduced doping which can lead to lower dark current and improvement in the quality of material. The detection mechanism of the HEIWIP detector involves absorption in the doped emitter layers of GaAs, mainly by free carriers, followed by the internal photoemission of photoexcited carriers across the work function at the $Al_xGa_{1-x}As$ barrier followed by collection. By adjusting the Al fraction, the cutoff wavelength λ_c can be tailored to the desired value.[3] The doping level in the GaAs emitters of the GaAs/AlGaAs structures should be high enough (typically around $3-5\times10^{18}$ cm^{-3}) for infrared absorption, but should not be so high as to cause excess dark current. It has been shown that the free carrier absorption remains high up to ~200 μm and may even be significantly increased by appropriate design architecture.[4]

In this article, the infrared absorption in the range of 5–100 μm (3–60 THz) for HEIWIP structures is presented and the effect of the structure thickness is demonstrated.

II. EXPERIMENT

Three detector samples with different thickness were used for reflection and transmission measurements. Structures were grown by molecular-beam epitaxy on 400 μm thick semi-insulating GaAs substrate. After growing 20 periods of a GaAs(20 Å)/AlAs(20 Å) superlattice as a buffer layer, multilayer device structures were grown. A multilayer structure consists of a highly Be-doped bottom contact layer of thickness W_{bc}, N periods of 800 Å thick $Al_{0.02}Ga_{0.98}As$ undoped barrier layer (W_i), followed by 158 Å thick Be-doped GaAs emitter layer (W_e), and a highly Be-doped top contact layer (W_{tc}). The samples 2409; 2283, and 2282 contained 30, 19, and 13 periods, respectively. N periods of GaAs/AlGaAs layers will give $N+1$ emitters due to the partial top contact layer. The layer parameters of the samples, confirmed by secondary ion mass spectroscopy (SIMS), are presented in Table I.

The structure of the front-illuminated HEIWIP detector is shown in Fig. 1. The devices were processed by etching 400×400 μm^2 mesas using a wet etching technique and then evaporating Ti/Pt/Au ohmic contacts onto the top and bottom contact layers. A 260×260 μm^2 window was opened through the top contact to provide front illumination to the device. The top contact thickness in the window was about few hundred angstroms.

The reflection and transmission spectra were measured at room temperature with a Perkin–Elmer system 2000 Fourier transform infrared (FTIR) spectrometer in the spectral range of 5–100 μm (3–60 THz) with an optical resolution of 4 cm^{-1} (0.12 THz). The incident angle in the reflection measurement was ~10°. Absorption spectra were calculated as the difference between unity and the sum of the reflection and transmission spectra. The responsivity spectra of the devices were measured using the FTIR spectrometer and a silicon bolometer as the reference detector.

a)Electronic mail: uperera@gsu.edu

TABLE I. Main parameters for three device structures. Here, W_{bc} and W_{tc} are the thicknesses of the bottom and top contacts (p^{++}). Thickness of emitter (p^{+})—158 Å and intrinsic (i) barrier layer—800 Å are the same for all structures. N_{bc}, N_{tc}, and N_e are the doping concentrations of the bottom and top contacts and emitter layer respectively. N is the number of periods of GaAs/AlGaAs layers, giving $N+1$ emitters.

Sample number	W_{bc} (nm)	N_{bc} 10^{19} cm^{-3}	W_{tc} (nm)	N_{tc} 10^{19} cm^{-3}	N_e 10^{19} cm^{-3}	N periods
2409	730	2.4	208	2.4	0.2	30
2283	660	0.9	360	0.9	0.4	19
2282	540	0.8	380	0.8	0.4	13

III. THEORY

The reflection and transmission can be calculated by introducing the complex refractive index n_j and complex permittivity ε_j [according to $n_j=\sqrt{\varepsilon_j(\omega)}$] of the jth layer in the structure. In order to simplify calculations, multiphonon absorption was not considered. According to the Drude model for free carriers and the multioscillator model for optical phonons:[5]

$$\varepsilon_j(\omega)=\varepsilon_{\infty,j}\left[1-\frac{\omega_{p,j}^2}{\omega(\omega+i\omega_{0,j})}\right]+\frac{\omega_{\mathrm{TO},j}^2(\varepsilon_{s,j}-\varepsilon_{\infty,j})}{\omega_{\mathrm{TO},j}^2-\omega^2-i\omega\gamma_j}. \tag{1}$$

Here, the first term describes the interaction between the free carriers and electromagnetic wave with frequency ω, $\omega_0=1/\tau$ is the free carrier damping constant with a relaxation time of τ, $\omega_p=\sqrt{N_p q^2/\varepsilon_o\varepsilon_s m^*}$ is a plasma frequency of free carriers with effective mass m^* and concentration N_p, ε_s is the static dielectric constant of the intrinsic semiconductor, and q is the magnitude of the electron charge. The second term in Eq. (1), the ''restrahlen'' term, describes the interaction with optical phonons in the frame of the Lorenz model. Here, ε_∞ is the high-frequency dielectric constant, ω_{TO} is the transverse optical (TO)-phonon frequency, and γ is a damping coefficient.

In the calculations, the following parameters were used for GaAs and $Al_{0.02}Ga_{0.98}As$: $\varepsilon_s=12.85$, $\varepsilon_\infty=10.88$, $\hbar\omega_{\mathrm{TO}}=33.25$ meV, and $\hbar\gamma=0.25$ meV as in Ref. 4. The relaxation time is $\tau=1.2\times10^{-14}$ s in accordance with the value recently used[4] for carbon-doped layers and is similar to 1.7×10^{-14} s obtained for a beryllium-doped GaAs layers.[6] For the AlAs buffer layers: $\varepsilon_s=10.0$, $\varepsilon_\infty=8.15$, longitudinal optical (LO)-phonon energy $\hbar\omega_{\mathrm{LO}}=50.1$ meV were used.[7] The TO-phonon frequency was calculated from the Lyddane–Sachs–Teller relation $\omega_{\mathrm{TO}}=\omega_{\mathrm{LO}}\sqrt{\varepsilon_\infty/\varepsilon_s}$.

The light propagation through a multilayer structure can be described by the matrix method.[8] There are two waves with electric-field amplitudes E^+ and E^- propagating in opposite directions in each layer. The boundary condition for electric and magnetic fields on the surface between two layers with complex refractive index n_{j-1} and n_j leads to the matrix T_j describing light penetration from $(j-1)$th layer to (j)th layer:

$$\begin{pmatrix}E_j^+\\E_j^-\end{pmatrix}=\frac{1}{2}\begin{pmatrix}1+n_{j-1}/n_j & 1-n_{j-1}/n_j\\1-n_{j-1}/n_j & 1+n_{j-1}/n_j\end{pmatrix}\cdot\begin{pmatrix}E_{j-1}^+\\E_{j-1}^-\end{pmatrix}=T_j\cdot\begin{pmatrix}E_{j-1}^+\\E_{j-1}^-\end{pmatrix}. \tag{2}$$

Light propagation in the jth layer with thickness d_j is described by the matrix:

$$D_j=\begin{pmatrix}\exp(i2\pi k(\omega)n_j d_j) & 0\\0 & \exp(-i2\pi k(\omega)n_j d_j)\end{pmatrix}. \tag{3}$$

Here, $k(\omega)=\omega/2\pi c$ is the wave number and c is the speed of light in a vacuum. The propagation through the whole structure is described by the matrix Q:

$$\begin{pmatrix}E_{\mathrm{out}}^+\\E_{\mathrm{out}}^-\end{pmatrix}=\Pi(D_jT_j)\cdot\begin{pmatrix}E_{\mathrm{in}}^+\\E_{\mathrm{in}}^-\end{pmatrix}=Q\cdot\begin{pmatrix}E_{\mathrm{in}}^+\\E_{\mathrm{in}}^-\end{pmatrix}. \tag{4}$$

The transmission $\mathcal{T}$ and reflection $\mathcal{R}$ coefficients may be found from the condition that at ''infinity,'' there is no return wave, and so $E_{\mathrm{out}}^-=0$. That leads to

$$\mathcal{R}=\left|\frac{Q_{2,1}}{Q_{2,2}}\right|^2;\quad \mathcal{T}=\left|\frac{\det(Q)}{Q_{2,2}}\right|^2. \tag{5}$$

The calculated spectra were averaged over the spectral interval with a resolution of 4 cm^{-1} (0.12 THz) to match the resolution of experimental spectrum.

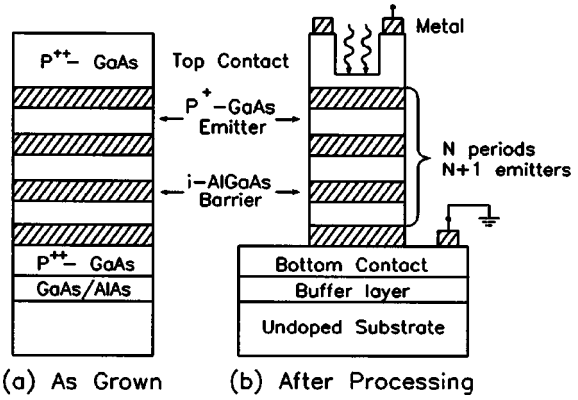

FIG. 1. The device structures (a) as grown and (b) after being processed. The (p^+) doped GaAs constitutes the emitter/absorber regions, while undoped AlGaAs layers constitute the barriers. Doping concentration and layer thickness are presented in Table I. Buffer layer is a 20 period GaAs/AlAs superlattice.

IV. RESULTS AND DISCUSSION

Figure 2 shows the experimental and calculated absorption (and reflection in the inset) spectra of the samples. Both, the experimental and theoretical absorption spectra were calculated from the expression $\mathcal{A}=1-\mathcal{T}-\mathcal{R}$. The period of the oscillation of the calculated spectra and positions of the extrema on the curves were fitted to the experimental data by varying the thickness of the layers. The best fits were obtained when the thicknesses from Table I were decreased by 5%, 4%, and 4% for samples 2409, 2283, and 2282, respectively. The fitting values lie in the range of SIMS measurement accuracy, considering the fact that sample 2409 was grown in a different run while 2283 and 2282 were grown together. The resonance cavity effect, which gives rise to absorption peaks, is seen in these structures, especially for the sample 2409 [see Fig. 2(a)]. This effect was due to the

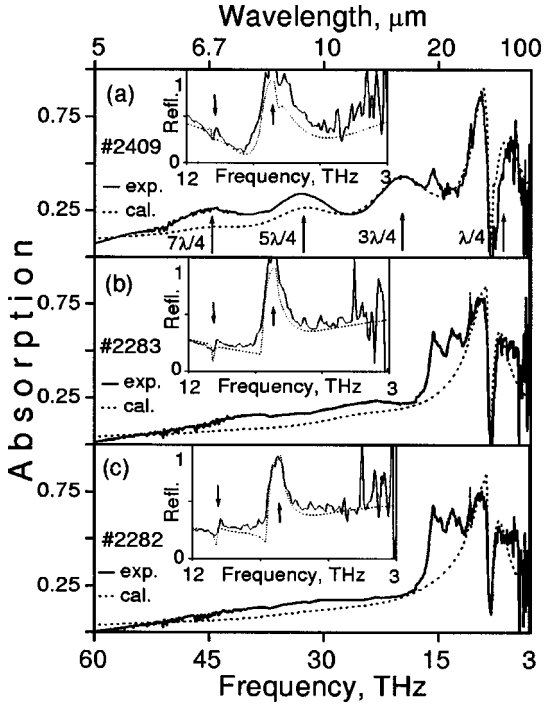

FIG. 2. The experimental (solid line) and calculated (dotted line) absorption spectra for the samples with different number of periods: (a) $N=30$, (b) $N=19$, and (c) $N=13$. Vertical arrows indicate the λ/4, 3λ/4, 5λ/4, and 7λ/4 absorption resonance peaks due to cavity effects. Insets show enlarged 3–12 THz reflection region with the restrahlen band of GaAs at 37 μm (8.1 THz) and spike at 27 μm (11.1 THz) due to AlAs presence emphasized by arrows.

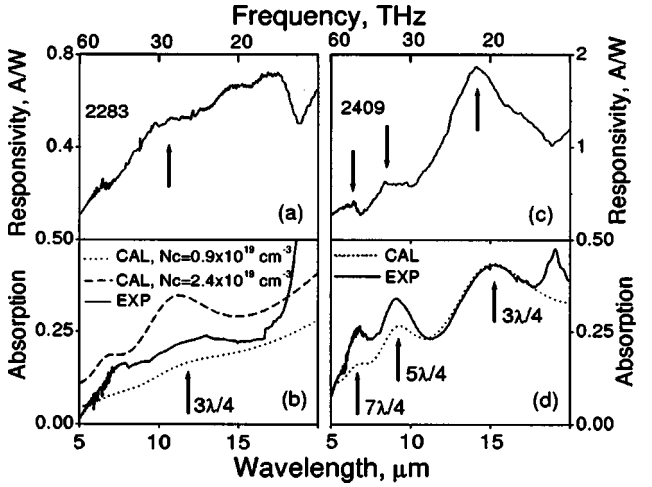

FIG. 3. The measured responsivity and absorption for samples 2283 [(a) and (b)] and 2409 [(c) and (d)] in the range of 5–20 μm showing the cavity enhancements at 6.5, 8.5, and 15.2 μm expected in 2409 and the smooth behavior expected in 2283. Dashed line in (b) demonstrates strong cavity effect with increased contact doping.

Fabry–Pérot interference between the light beams reflected mainly from highly doped top and bottom contact layers. At resonance,

$$\sum_j \mathrm{Re}(n_j(\lambda))d_j=(\lambda/4)(2m+1), m=0,1,2..., \qquad (6)$$

where $\mathrm{Re}(n_j)$ is the real part of the refractive index of the jth layer, d_j is its thickness, and the summation is carried throughout all the layers of the structure. At resonance, reflection decreases thereby increasing the absorption. The resonance enhancement for the FIR photodetector response based on this structure is expected to occur at wavelengths found from Eq. (6). The absence of the peaks on the curves for samples 2283 [see Fig. 2(b)] and 2282 [see Fig. 2(c)] is due to low doping concentrations in the contacts. As will be shown later, the skin depth for p type in wavelength region of 10–20 μm is about 10–100 μm—that is much longer than the bottom contact thickness. Due to the undoped substrate, the IR radiation travels through with weak reflection, consequently minimizing the cavity effect. The absorption peaks in the experimental curve in the range of 15–25 μm were caused by two-phonon absorption[9] not included in the theoretical model.

The reflection spectra behavior in the range of 25–100 μm (3–12 THz) seen in the inset of Fig. 2 is completely described by the plasmon–phonon resonance. The reflection maximum at the wavelength 37 μm (8.1 THz) is caused by the strong light interaction with phonons in GaAs. The spike at 27 μm (11.1 THz) shows the light interaction with LO phonons in AlAs, even though the AlAs layers are limited to only 400 Å (20 periods of 20 Å). Such behavior of the reflection spectra of $Al_xGa_{1-x}As$ has been observed before.[10] There are no sharp features in the spectra caused by the buffer layer owing to the small total thickness of the superlattice as compared to the wavelength. However, the best agreements with the experiment were achieved when the buffer layers were taken into account in the calculation.

Figure 3 shows the responsivity and absorption of samples 2283 and 2409 at 4.2 K in the wavelength range of 5–20 μm (15–60 THz). The response for sample 2409 [see Fig. 3(c)] shows maxima at 15.2, 8.5, and 6.5 μm corresponding to the 3λ/4, 5λ/4, and 7λ/4 maxima seen in Fig. 2(a). A small shift of the response peaks as compared with the absorption spectra [see Fig. 3(d)] is due to the thickness reduction after processing since most of the top contact layer was etched. Due to the rapid decrease in photoemission with wavelength and the presence of the restrahlen reflection maximum near 45 μm, the λ/4 peak was not clearly observed although there was a maximum around 33 μm that can be attributed to a combination of the photoemission, restrahlen reflection, and cavity effect. The responsivity of the device is regulated not only by the photon absorption but also by the collection of hot holes generated by absorbed photons, internal photoemission, and hot hole transport. The reduced enhancement of the cavity peaks at a short-wavelength region (5–10 μm) in the responsivity spectrum [see Fig. 3(c)] compared to absorption spectrum [see Fig. 3(d)] may be explained by the energy dependent hot hole relaxation processes in the emitters.[11]

The responsivity spectra [see Fig. 3(a)] for sample 2283 do not show any clear maxima associated with the cavity effect in accordance with absorption calculation and measurement [see Fig. 2(b)]. By increasing the bottom contact doping to 2.4×10^{19} cm^{-3}, one could see cavity peaks in the model as expected [dashed line for calculated absorption in Fig. 3(b)].

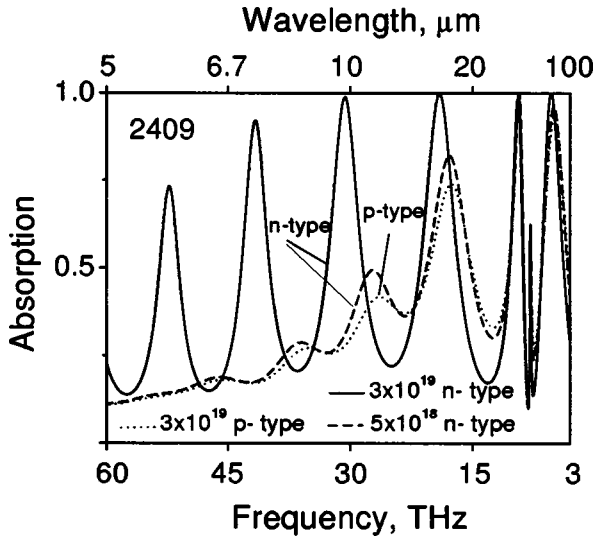

FIG. 4. Total absorption in a structure similar to sample 2409 with single 1 μm thick *p*-type (concentration 3×10^{19} cm^{-3}) GaAs buffer layer (dotted line). Absorptions for structure with *n*-type buffer with different concentrations are shown (dashed line—5×10^{18} cm^{-3} and solid line—3×10^{19} cm^{-3}). The shift of the peaks is due to the change in the skin depth in the buffer layer and consequently the effective thickness of the structure.

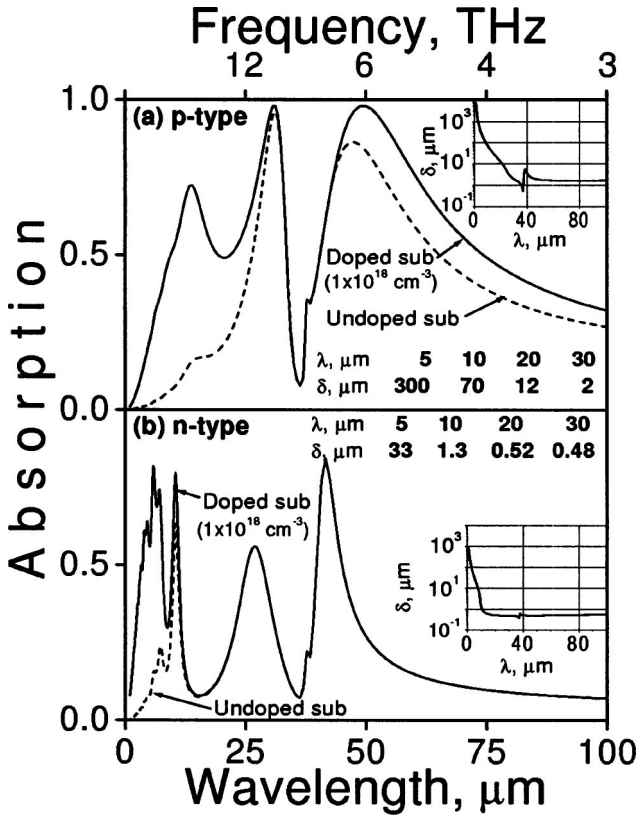

FIG. 5. Calculated total absorption in a GaAs/AlGaAs structure with (a) *p*-type and (b) *n*-type substrate and bottom contacts. Solid line—doped substrate (1×10^{18} cm^{-3} in both cases), and dashed line—undoped substrate. Top and bottom contacts doping level—1×10^{19} cm^{-3}. Thickness of emitter —188 Å, intrinsic barrier layer—1250 Å, bottom contact—1.5 μm, and substrate—400 μm. $N_e=3\times10^{18}$ cm^{-3}. Number of periods of GaAs/AlGaAs layers is 12. Insets show skin depth δ variation with wavelength λ for *p*- and *n*-type substrates.

All layers contribute to the formation of standing waves in the structure, including the ''buried'' layers under the bottom contact (GaAs/AlAs buffer layers). These layers work as mirrors—they do not take part in the injection of carriers and other electrical phenomena. Growing such layers with proper parameters (thickness, doping level, etc.), in combination with other layers, may increase the electric field in the injection layers and thus enhance FIR detector performance.

Figure 4 demonstrates the expected influence of concentration and type of doping on the total absorption in a structure similar to 2409 due to a 1 μm thick GaAs n^{++}- and p^{++}-type buffer layer. At the same doping level, the n^{++}-type reflects IR radiation more effectively than the p^{++} type due to a smaller effective mass of electrons as compared to the mass of a hole. It is clear that by varying the thickness of the structure and the concentration of the buffer region, one can tailor the detector peaks to desired wavelengths. In fact, the present p^{++}-type contact layer can be changed to a n^{++}-type layer without increasing the total thickness of the device structure. The presence of a *p*-*n* junction will not affect the device performance at forward bias, and may even reduce the dark current.

A structure with a doped substrate may be used for a processed front-illuminated device. Figure 5 shows the comparison of the absorption spectra of GaAs/AlGaAs structure with doped (*n* and *p* type) and undoped substrates. The structure consists of 12 periods of emitter/barrier layers and the top and bottom contacts. The emitter layer thickness is 188 Å, while the barrier layers are 1250 Å thick. The top and bottom contacts are 200 Å and 1.5 μm, respectively. The substrate thickness is around 400 μm. The doping level of the emitters is 3×10^{18} cm^{-3}, contact layers—1×10^{19} cm^{-3}, and substrate—1×10^{18} cm^{-3}.

It is shown that for a *p*-type bottom contact layer and substrate [see Fig. 5(a)], the skin depth δ [see inset in Fig. 5(a)] is larger than the bottom contact thickness for wavelengths $\lambda\leqslant30$ μm. This indicates that the reflection, which forms the cavity resonance, takes place inside the substrate. At a short wavelength, the skin depth is comparable with the substrate thickness which leads to reflection reduction. For *n* type [see Fig. 5(b)], the reflection forming cavity resonance for wavelengths longer than 8 μm takes place in the contact region. At shorter wavelengths, strong reflection takes place inside the substrate. In general, shorter wavelengths have longer skin depths making the substrate doping important. The minimum seen around 10 μm [see Fig. 5(b)] in the calculated absorption curve for a *n*-type substrate is due to the changes in the resonance cavity condition since the refractive index has a minimum at this wavelength. The complicated behavior of the absorption spectrum at shorter wavelengths is due to the refractive index change (from 3.3 to 0.3 in the 1–10 μm range for *n* type) and, hence, the change in resonance cavity condition. For the same wavelength region, for a *p*-type substrate, the change in the refractive index is almost negligible. Figures 5(a) and 5(b) demonstrate the possibility for adjustment of the cavity peak resonance at desired wavelengths by varying the substrate type and doping level without growing an additional buffer layer.

V. CONCLUSION

In summary, the reflection, absorption, and responsivity of the structures with a different number of Be-doped GaAs/AlGaAs layers are presented. Experimental and calculated results are in good agreement indicating that the behavior can be explained by the free carrier absorption and interaction with optical phonons. It has been demonstrated that the resonance cavity architecture could be used to improve the responsivity at specific wavelengths. The position and strength of the absorption peaks may vary by varying the thickness and doping level of the structure. Using the n^{++} buffer as a bottom contact further increases the responsivity at a designed wavelength.

ACKNOWLEDGMENTS

This work was supported in part by the NSF under Grant No. ECS-01-40343 and the Department of National Defense, Canada. One of the authors M. B. M. R. was supported, in part, by the GSU RPE funds. The authors thank P. Chow-Chong and P. Marshall for microfabrication, G.I. Sproule for SIMS measurements, and N. Zelikovskaya for technical support.

[1] A. G. U. Perera, in *Semiconductor Optics*, Handbook of Thin-Film Devices Frontiers of Research, Technology, and Applications Vol 2, edited by M. H. Francombe, A. G. U. Perera, and H. C. Liu (Academic, New York, 2000), pp. 135–169.
[2] A. G. U. Perera, S. G. Matsik, B. Yaldiz, H. C. Liu, A. Shen, M. Gao, Z. R. Wasilewski, and M. Buchanan, Appl. Phys. Lett. **78**, 2241 (2001).
[3] S. G. Matsik, M. B. M. Rinzan, A. G. U. Perera, H. C. Liu, Z. R. Wasilewski, and M. Buchanan, Appl. Phys. Lett. **82**, 136 (2003).
[4] A. L. Korotkov, A. G. U. Perera, W. Z. Shen, J. Herfort, K. H. Ploog, W. J. Schaff, and H. C. Liu, J. Appl. Phys. **89**, 3295 (2001).
[5] J. S. Blakemore, J. Appl. Phys. **53**, R123 (1982).
[6] M. L. Huberman, A. Ksendzov, A. Larsson, R. Terhune, and J. Maserjian, Phys. Rev. B **44**, 1128 (1991).
[7] S. Adachi, J. Appl. Phys. **58**, R1 (1985).
[8] M. V. Klein and T. E. Furtac, *Optics* (Wiley, New York, 1986).
[9] E. S. Koteles and W. R. Datars, Can. J. Phys. **54**, 1676 (1976).
[10] M. Ilegems and G. L. Pearson, Phys. Rev. B **1**, 1576 (1970).
[11] A. G. U. Perera, H. X. Yuan, and M. H. Francombe, J. Appl. Phys. **77**, 915 (1995).